Phonon-induced Raman processes connecting the $\bar{E}(^2E)$ and $2\bar{A}(^2E)$ states in ruby

R. J. G. Goossens,* J. I. Dijkhuis, and H. W. de Wijn
Fysisch Laboratorium, Rijksuniversiteit Utrecht, P.O. Box 80.000, 3508 TA Utrecht, The Netherlands
(Received 22 April 1985)

The dynamics of near-zone-boundary phonons is investigated in ruby at low temperature by use of a technique of modulated pumping. The phonons are generated in the nonradiative decay to ^2E following optical excitation of $^4T_1$ or $^4T_2$. The detection is via phonon-induced Raman transitions from $\bar{E}(^2E)$ to $2\bar{A}(^2E)$, and the associated enhancement of the R_2 luminescence. The phonon occupation is linear in the optical-pumping intensity, but becomes quadratic in case of significant secondary optical pumping starting from the ^2E states, and reaches values of up to 10^{-7}. The prevailing decay mechanism appears to be ballistic flight out of the pumped zone over distances of up to 0.3 mm, corresponding to lifetimes of over 200 ns. An additional result is the optical feeding constant into $2\bar{A}(^2E)$.

I. INTRODUCTION

During the last few years there has been considerable debate on the lifetime of near-zone-boundary phonons. Experiments in quartz,[1] and recently in GaAs (Refs. 2 and 3) and TlCl,[4] all point to long lifetimes (up to 1 μs) and large distances of travel (up to 1 mm). Indeed, by quite general theoretical arguments near-zone-boundary phonons of the lowest acoustic branch cannot decay by anharmonic processes,[5] which in the case of perfectly translation-invariant crystals would infer infinitely long lifetimes. In real crystals, however, mode conversion induced by impurities, defects, and isotopes would presumably limit the intrinsic lifetime by a breakup into rapidly decaying modes at lower frequencies. In this paper we present experiments on near-zone-boundary acoustic phonons taking advantage of optically pumped Cr^{3+} centers in diluted ruby. The results point to surprisingly long lifetimes by ballistic motion, and consequently weak mode conversion. The phonons are generated by the breakup of the energy associated with the nonradiative decay following optical pumping, and detected by the enhancement of the R_2 luminescence due to Raman transitions invoked by these phonons. The rate of these transitions is in fact directly accessible to experimental examination by measuring the total feeding in $2\bar{A}(^2E)$ via the modulated pumping scheme employed here. The Raman processes connecting $2\bar{A}(^2E)$ and $\bar{E}(^2E)$ also bear on the discrepancy between earlier continuous-wave[6] and time-resolved[7,8] experiments on 29-cm^{-1} phonons, as was first noted by Basun *et al.*[9] Additional feeding into $2\bar{A}(^2E)$ turns out to drive the hot 29-cm^{-1} phonon spike several orders of magnitude above the value expected from the measured relaxation time of $2\bar{A}(^2E)$ and the rate of the optical-pumping cycle alone. This effect, as will become clear below, is entirely due to the optical generation and the longevity of near-zone-boundary phonons. The above findings have been corroborated, in a separate paper,[10] by independent measurements in ruby of the Raman transition rate induced between the Zeeman components of $\bar{E}(^2E)$ in an external magnetic field. Finally, the feeding rate of the optical pumping into $2\bar{A}(^2\bar{E})$ is determined.

II. INTERPRETATION OF EXPERIMENTS WITH MODULATED PUMPING

The technique of modulated pumping allows one to determine in a single experiment, i.e., at identical total metastable concentration N^*, (i) the equilibrium population of the metastable levels that would be maintained under the conditions of continuous pumping, and (ii) the decay time of these levels as measured in a time-resolved experiment. When applied to the case of the metastable $\bar{E}(^2E)$ and $2\bar{A}(^2E)$ states of ruby (Fig. 1) at low temperatures ($\sim$1.5 K), modulated pumping implies a repetition period short compared to the radiative lifetime (τ_R=3.7 ms), but long compared to the decay time T_{eff} of $2\bar{A}(^2E)$

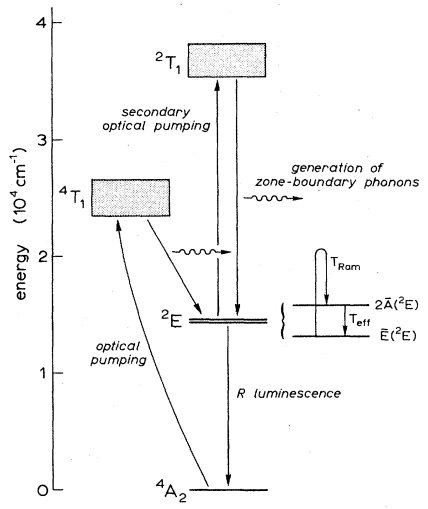

FIG. 1. Schematic energy-level diagram of Cr^{3+}:Al_2O_3. Near-zone-boundary phonons are generated in the nonradiative decays following primary and secondary optical pumping. These phonons induce additional feeding into $2\bar{A}(^2E)$ by Raman transitions starting from $\bar{E}(^2E)$. Resonant 29-cm^{-1} phonons are produced in the one-phonon decay $2\bar{A}(^2E)$ to $\bar{E}(^2E)$ with a time constant T_{eff}, elongated by bottlenecking. Diagram applies to pumping with the 458-nm argon line; at 514 nm, pumping is primarily to the $^4T_2$ band located around 18 000 cm^{-1}, while no efficient secondary pumping occurs.

($T_{\text{eff}} < 3$ μs, dependent on the conditions). Accordingly, repetition rates as high as 200 kHz are feasible. Under these conditions, a virtually constant N^* is produced, corresponding to the average pumping intensity (note that $N_{\bar{E}} \approx N^*$). The equilibrium ratio of populations may then be derived from the R_2 and R_1 emissions, while T_{eff} is retrieved from the decay of R_2 following removal of the optical pumping.

The rate of the Raman processes connecting $\bar{E}(^2E)$ and $2\bar{A}(^2E)$ induced by optically generated near-zone-boundary phonons[11] is now accessible by combining the population ratio and T_{eff}. To demonstrate this point, we write down the rate equations of the Cr^{3+} populations $N_{\bar{E}}$ and $N_{2\bar{A}}$ in the metastable states, and the occupation number p of the resonant 29-cm^{-1} phonons. That is,

$$\begin{aligned}
\frac{dN_{\bar{E}}}{dt} &= \frac{(p+1)N_{2\bar{A}} - pN_{\bar{E}}}{T_d} + \frac{p_{\text{ZB}}(N_{2\bar{A}} - N_{\bar{E}})}{T_{\text{Ram}}} \\
&\quad - \frac{N_{\bar{E}}}{\tau_R} + \Phi_{\bar{E}}\eta(t) , \\
\frac{dN_{2\bar{A}}}{dt} &= \frac{-(p+1)N_{2\bar{A}} + pN_{\bar{E}}}{T_d} + \frac{p_{\text{ZB}}(N_{\bar{E}} - N_{2\bar{A}})}{T_{\text{Ram}}} \\
&\quad - \frac{N_{2\bar{A}}}{\tau_R} + \Phi_{2\bar{A}}\eta(t) , \qquad (1) \\
\rho\Delta\nu\frac{dp}{dt} &= \frac{(p+1)N_{2\bar{A}} - pN_{\bar{E}}}{T_d} - \frac{\rho\Delta\nu p}{\tau} ,
\end{aligned}$$

in which T_d is the spontaneous direct transition time of $2\bar{A}(^2E)$ to $\bar{E}(^2E)$, p_{ZB} is the occupation number of the near-zone-boundary phonons averaged over the modes active in Raman transitions, T_{Ram} is the effective time constant of the Raman processes, $\Phi_{\bar{E}}\eta(t)$ and $\Phi_{2\bar{A}}\eta(t)$ represent the optical feeding, ρ is the density of the resonant phonon modes, and $\Delta\nu$ is the width of the resonant phonon packet; $\eta(t)=1$ during optical pumping, and $\eta(t)=0$ in the light-off period. We have, for simplicity, assumed the phonon decay to be described by a linear loss term with a unique time constant τ. The time constant T_{Ram} contains all relevant details of the Raman processes, and has been estimated in a calculation connecting the rates of these processes to T_d with the result $T_{\text{Ram}} \approx 10^{-10}$ s.[10]

We solve Eqs. (1) under the conditions of strong bottlenecking of the 29-cm^{-1} phonons ($\sigma = N^*\tau/\rho\Delta\nu T_d \gg 1$), negligible radiative decay ($\tau_R \gg T_{\text{eff}}$), and light-on and light-off periods longer than T_{eff} but shorter than τ_R, to obtain for the time-averaged excited-state population ratio

$$\langle N_{2\bar{A}} \rangle / N_{\bar{E}} = \langle (\phi_{2\bar{A}} + p_{\text{ZB}}/T_{\text{Ram}}) \rangle \sigma T_d , \qquad (2)$$

with $\langle \phi_{2\bar{A}} \rangle = \langle \Phi_{2\bar{A}} \rangle / N^*$, and for the decay time of R_2 following removal of the feeding

$$T_{\text{eff}} = \sigma T_d (1 + \rho\Delta\nu/N^*) . \qquad (3)$$

In connection with Eq. (2), we point out that, because $N_{2\bar{A}} \ll N_{\bar{E}}$, the Raman process may alternatively be envisaged as an additional feeding into $2\bar{A}(^2E)$ of magnitude $p_{\text{ZB}}/T_{\text{Ram}}$, or

$$\phi_{2\bar{A}}^{\text{tot}} = \phi_{2\bar{A}} + p_{\text{ZB}}/T_{\text{Ram}} . \qquad (4)$$

Combining Eqs. (2) and (3), and noting that in all experimental situations encountered here $\rho\Delta\nu/N^* \ll 1$ ($\rho\Delta\nu = 4\times10^{16}$ cm^{-3} for transverse acoustic phonons), we finally arrive at

$$\langle \phi_{2\bar{A}}^{\text{tot}} \rangle = \frac{\langle N_{2\bar{A}} \rangle}{N_{\bar{E}} T_{\text{eff}}} . \qquad (5)$$

Equation (5) expresses that the basic information to be retrieved from the two quantities measured in the modulated pumping experiments, $\langle N_{2\bar{A}} \rangle / N_{\bar{E}}$ and T_{eff}, is the total feeding into $2\bar{A}(^2E)$. It should be emphasized that this result is to a large extent independent of the particular mechanism of the phonon decay, since Eq. (5) merely reflects a balancing of the processes governing the $2\bar{A}(^2E)$ population. Even such a fundamental modification of Eqs. (1) as the replacement of the phonon loss mechanism adopted by pure boundary-limited spatial diffusion[6] does not affect the functional dependence of Eq. (5), although it adds a multiplicative factor of 0.72 on the right-hand side. With regard to the sensitivity of the scheme for the detection of near-zone-boundary phonons, we see that the Raman-induced feeding is already of the order of the direct optical feeding for p_{ZB} as low as 10^{-9} (an upper limit of $\phi_{2\bar{A}}$ is $1/\tau_R$).

III. EXPERIMENTAL RESULTS AND DISCUSSION

In this section we present measurements on the total feeding into the $2\bar{A}(^2E)$ levels, $\phi_{2\bar{A}}^{\text{tot}}$, for three different ruby samples. By use of atomic absorption, the Cr^{3+} ground-state concentrations for these crystals were determined to be 130, 700, and 2500 at. ppm.[12] The crystals have the form of thin slabs (thickness 0.3, 0.4, and 0.2 mm, respectively). The excitation was accomplished with an argon laser operating either in the single-line mode at 514 or 458 nm, or in the all-lines mode (5 W maximum output). The laser beam was chopped by an acousto-optical modulator, achieving rise and fall times of better than 30 ns. The R_1 and R_2 emissions were detected with a double monochromator and standard photon-counting techniques. The temporal evolution of the intensities was determined by use of a time-to-amplitude converter. All measurements were done at low temperature (1.5 K) to eliminate relaxation by thermal phonons. For further details, including those pertaining to the numerical analysis of the decays leading to T_{eff}, one is referred to Ref. 13.

A. Raman feeding versus N^*

To illustrate the technique, and also to discuss the origin of p_{ZB}, we first present some representative data on the 700—at. ppm sample taken with a laser beam with radius $R = 200$ μm, i.e., such low N^* that $\phi_{2\bar{A}}$ and $p_{\text{ZB}}/T_{\text{Ram}}$ are of similar magnitude. Figure 2 shows both $\langle N_{2\bar{A}} \rangle / N_{\bar{E}}$ and T_{eff} versus N^*, where by virtue of the modulated pumping scheme the abscissas are automatically tied together. These data reworked to $\phi_{2\bar{A}}^{\text{tot}}$ according to Eq. (5) are presented in Fig. 3. A linear increase with N^*

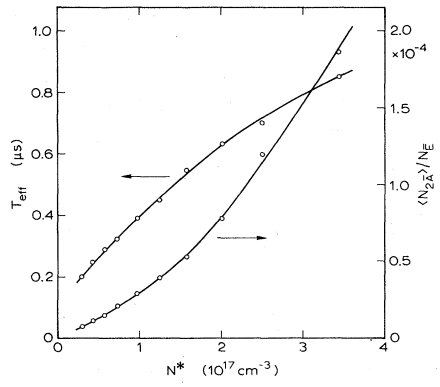

FIG. 2. T_{eff} and $N_{2\bar{A}}/N_{\bar{E}}$, as determined by the modulated pumping technique, vs N^* in 700—at. ppm ruby at 1.5 K with optical pumping at 514 nm. The excited zone is a cylinder with radius 200 μm. The N^* scale has limited accuracy only. Data have been corrected for reabsorption of the luminescence.

is observed, intersecting the ordinate at $\phi_{2\bar{A}} = 19 \pm 10\ \text{s}^{-1}$, with the error mainly residing in a correction for reabsorption. It is noted that similar results for $\phi_{2\bar{A}}^{\text{tot}}$ in the 130— and 2500—at. ppm samples, not presented here, also exhibit a linear rise vs N^*. All data taken together, we arrive at $\phi_{2\bar{A}} = 20 \pm 5\ \text{s}^{-1}$.[14]

The most prominent result borne out by Fig. 3 is the linearity of p_{ZB} on N^*, justifying the assumptions leading to incorporating terms of the form $p_{\text{ZB}}(N_{\bar{E}} - N_{2\bar{A}})/T_{\text{Ram}}$ in Eqs. (1). Thus, the optically produced near-zone-boundary phonon occupation appears to be proportional to the pumping intensity. In working this out in somewhat more detail, we estimate the number of phonons produced as follows. The excess energy of the optical-pumping cycle released in the nonradiative decay from the broadbands amounts to about 5000 cm^{-1} at 514 nm, and ultimately has to be taken up by the acoustic phonons, presumably more or less uniformly distributed over all

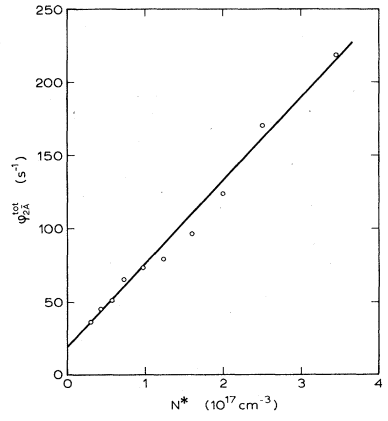

FIG. 3. Total feeding into $2\bar{A}(^2E)$, $\phi_{2\bar{A}}^{\text{tot}}$, in 700—at. ppm ruby at 1.5 K vs N^*, derived from the data in Fig. 2. Intercept at $N^* = 0$ represents the direct optical feeding, and the linear increase represents the Raman transition rate of $\bar{E}(^2E)$ to $2\bar{A}(^2E)$.

modes. The emphasis that the density of states puts on the region in **k** space near the zone boundary then ensures that the energy associated with the nonradiative decay preferentially ends up in phonons near the zone boundary, having an average energy of about 230 cm^{-1}. The feeding of near-zone-boundary phonons generated may thus be assessed to be

$$\Phi_{\text{ZB}} = \frac{1}{3N} \frac{N^*}{\tau_R} \frac{5000}{230}\ , \tag{6}$$

where $3N$ is the number of acoustic modes. For a typical $N^* = 10^{18}$ cm^{-3} in ruby, the feeding per mode equals $\Phi_{\text{ZB}} = 0.2\ \text{s}^{-1}$. Then, p_{ZB} of the transverse branches is determined by balancing the feeding into the near-zone-boundary phonons with their decay, which is assumed to be uniexponential with a unique decay time τ_{ZB}, or

$$p_{\text{ZB}} = \Phi_{\text{ZB}} \tau_{\text{ZB}}\ . \tag{7}$$

The longitudinal acoustic phonons have such short lifetimes ($\approx 10^{-11}$ s) as to be ineffective in Raman transitions. It is further noted that near-zone-boundary phonons are favored in effecting Raman transitions by the transition probability of the process, which approximately goes with $k^2 k'^2/\omega\omega'$, where ω is the angular frequency and the primed quantities refer to the outgoing phonon ($\hbar\omega - \hbar\omega' = 29\ \text{cm}^{-1}$).

Results for τ_{ZB} of the transverse phonons deduced with Eqs. (6) and (7) from the experimental $p_{\text{ZB}}/T_{\text{Ram}}$ are, to better accuracy than Fig. 3 permits, extracted from the data extended to higher N^* by focusing down the laser beam ($R = 25$ μm). The result for all three samples are, after subtraction of $\phi_{2\bar{A}}$, presented in Fig. 4. We first discuss the data with optical pumping at 514 nm. The pumping up to higher N^* allows a reliable calibration, with reference to the $^4A_2$ ground-state concentration, of the N^* scale versus the R_1 intensity by observing the de-

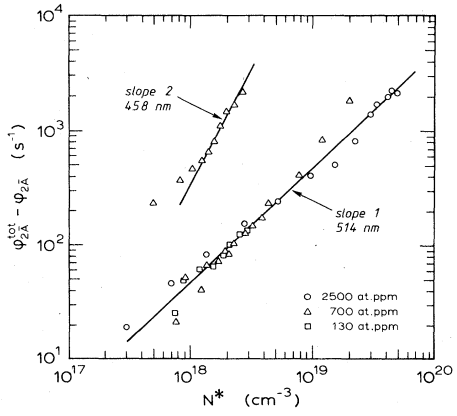

FIG. 4. Raman part of the feeding into $2\bar{A}(^2E)$, $\phi_{2\bar{A}}^{\text{tot}} - \phi_{2\bar{A}}$, in 130—, 700—, and 2500—at. ppm ruby at 1.5 K upon optical pumping at 514 or 458 nm. The excited zone has diameter 60 μm. Data for 700 and 2500 at. ppm are corrected for reabsorption. Slopes 1 and 2 point to generation of near-zone-boundary phonons in the primary and secondary optical-pumping cycles, respectively.

pletion of the ground state as reflected in the leveling off of the R_1 intensity versus laser power. The N^* scale determined in this way is to a large degree insensitive of the effects of reabsorption. We estimate the N^* scale to be accurate within 25%, apart from any systematic errors in the determination of the ground-state concentration. Further, the narrowing down of the laser beam permits smaller distances of travel of the R luminescences to the surface of the crystal, thus reducing the undesired effects of reabsorption on both the ratio R_2/R_1 and the R_1 intensity. In Fig. 4, the N^* scale being fixed, the 130—at. ppm data, for which reabsorption is negligible, are taken as a gauge for the ordinate. To correct for reabsorption in the 700- and 2500-at. ppm samples, the data in these samples as measured at 514 nm have subsequently been shifted downwards by factors of 1.3 and 1.7, respectively, to obtain coincidence in regimes of N^* for which data for all three concentrations are available. These factors are consistent with the results of independent measurements on the reabsorption in these samples in magnetic fields, while the corrections are in the right direction in view of the transition probabilities of R_1 and R_2 in the specific geometry. Returning to the interpretation of $\phi_{2\bar{A}}^{\text{tot}}-\phi_{2\bar{A}}$ (Fig. 4), we first observe this quantity to be linear in N^* over at least two decades, which confirms the assumed independency of τ_{ZB} on N^*, and thus rules out trapping of the phonons by excited Cr^{3+}. For $N^*=10^{18}$ cm^{-3} and an excited-zone radius $R=25$ μm, then, we find with Eq. (4) from Fig. 4 the result $p_{ZB}\approx 5\times 10^{-9}$, leading with the appropriate $\Phi_{ZB}\approx 0.2$ s^{-1} to $\tau_{ZB}\approx 25$ ns. This corresponds to an escape out of the excited zone at a velocity of approximately 10^5 cm/s, substantially below the velocity of sound, which is 6.4×10^5 cm/s. The latter result is, of course, subject to some uncertainty because of the approximations made in the calculation of T_{Ram} and Φ_{ZB}, but may nevertheless be regarded to constitute further evidence for the involvement of near-zone-boundary phonons.

B. Secondary optical pumping

In the preceding subsection the laser excitation was at 514 nm. Here, we consider excitation with the 458-nm line. In contrast to an 514-nm line, the 458-nm line falls near the center of an absorption band from the ^2E metastable states to still higher states. The resultant secondary pumping provides an additional generation of near-zone-boundary phonons, proportional to N^{*2} rather than N^*, provided a significant fraction of the Cr^{3+} ions is in the metastable states. By analogy with Eq. (6), the number of near-zone-boundary phonons generated is

$$\Phi_{ZB}=\frac{1}{3N}\left[\frac{N^*}{\tau_R}\frac{7400}{230}+\frac{\alpha_2}{\alpha_1}\frac{N^{*2}}{N_0\tau_R}\frac{21\,800}{230}\right], \tag{8}$$

where N_0 is the ground-state concentration, and α_1 and α_2 denote the cross sections for absorption of laser quanta by Cr^{3+} in the $^4A_2$ and $\bar{E}(^2E)$ states, respectively. For the polarization of the incident beam used here ($\mathbf{E}||c$ axis) $\alpha_2/\alpha_1\approx 40$ at 458 nm (cf. Ref. 15, with allowance for the reduction of α_1 by a factor of 4 upon cooling from 105 to 1.5 K). For comparison, for the same polarization $\alpha_2/\alpha_1=1$ at 514 nm. Accordingly, at 458 nm the phonon production is being taken over by the secondary pumping cycle above $N^*/N_0\approx 10^{-2}$, while at 514 nm $N^*/N_0\approx 0.3$ would be needed to achieve an equivalent effect.

Data of $\phi_{2\bar{A}}^{\text{tot}}-\phi_{2\bar{A}}$ versus N^* upon excitation at 458 nm are presented in Fig. 4 for 700-at. ppm ruby. To these data applies the same N^* calibration as in the 514-nm case, but the effects of reabsorption may differ to some extent because the tuning of the laser is inevitably accompanied by a displacement of the excited zone. Indeed, as expected from Eq. (8), a pure quadratic dependence is observed above $N^*\approx 10^{18}$ cm^{-3}, corresponding to $N^*/N_0\approx 3\times 10^{-2}$ at the appropriate N_0. It is of interest to note that the linear part of the 458-nm data, when compared with the 514-nm data with due account of the excess energies [cf. Eqs. (6) and (8)], yields a comparable τ_{ZB}. The transition of the 458-nm data to linear dependence occurs at an N^* that is too high by a factor of 2, but the disparity should not be considered to be beyond the inaccuracy of the data at the lowest N^*. At 514 nm, the transition from a linear to a quadratic N^* dependence is, according to a suitable analog of Eq. (8), not expected to occur until $N^*\approx 10^{19}$ cm^{-3} in 700-at. ppm ruby, and $N^*\approx 3\times 10^{19}$ cm^{-3} in the case of 2500 at. ppm.

C. Size dependence of τ_{ZB}

In this section we present experiments that give access to the dependence of the lifetime of near-zone-boundary phonons on the dimensions of the excited zone. Via the size dependence one would be able to distinguish between various possible decay mechanisms, such as mode conversion (τ_{ZB} independent of the dimensions), decay by ballistic flight (τ_{ZB} proportional to the average flight path L out of the zone), and decay by boundary-limited spatial diffusion ($\tau_{ZB}\propto L^2$). In Fig. 5, we present the results of measurements of the Raman transition rate for a selection of diameters of the pumped cylinder upon varying the position of the focusing lens ($R=30$—280 μm). The diameter of the zone was calculated from the known beam diameter by standard geometrical optics with a correction

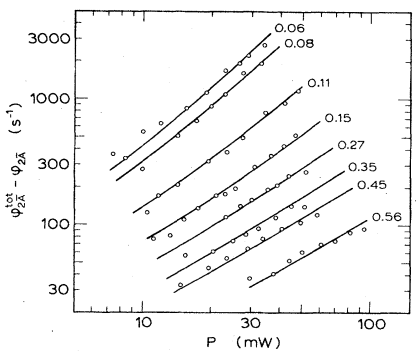

FIG. 5. Raman part of the feeding into $2\bar{A}(^2E)$, $\phi_{2\bar{A}}^{\text{tot}}-\phi_{2\bar{A}}$, in 700—at. ppm ruby at 1.5 K vs the laser power for various beam diameters, as indicated (in mm). Laser is operating in the all-lines mode. Solid lines represent a fit of Eq. (9) to the data, demonstrating τ_{ZB} to scale approximately with R.

for diffraction. To have efficient pumping also at the largest zone diameters, the laser was operated in the all-lines mode. For each diameter these measurements have been carried out as a function of the laser power to determine the effects of the secondary optical-pumping cycle with increasing N^*. Indeed, at small R a faster than linear increase of ϕ with laser power is observed, while at large R the increase is strictly linear.

To extract the L dependence of τ_{ZB}, we recall that $\phi_{2\bar{A}}^{tot}-\phi_{2\bar{A}}=\Phi_{ZB}\tau_{ZB}/T_{Ram}$, while N^* is proportional to the laser-power density $P/\pi R^2$. We further adopt at this point a power-law dependence of τ_{ZB} of the form $\tau_{ZB}\propto L^{\gamma}$, where the size dependence is contained in the exponent γ. Accordingly, we have

$$\phi_{2\bar{A}}^{tot}-\phi_{2\bar{A}}=\alpha\left[\frac{P}{\pi R^2}+\beta\left[\frac{P}{\pi R^2}\right]^2\right]R^{\gamma}, \tag{9}$$

where we have identified L with the cylinder radius R. The solid curves in Fig. 5 represent a fit of Eq. (9) to all data at the same time, with α, β, and γ as adjustable parameters. The quantity β is a measure of the contribution of the secondary pumping cycle. By extending Eq. (8) such as to include all appropriate laser lines and comparing Eq. (9) with the resultant expression, β may be related to $(N^*/N_0)/(P/\pi R^2)$, the relevant ratios α_2/α_1, and the ratio of the powers of the Ar lines. The result $\beta=2.7\times10^{-4}$ mm^2/mW calculated in this way appears to be consistent with the fitted result $\beta=(2.0\pm0.5)\times10^{-4}$ mm^2/mW within the uncertainties. The value for β shows that the data in Fig. 5 have entered the regime quadratic in P at the higher laser powers and the smaller diameters. As regards γ, with inclusion of the errors propagated from L and P, and a minor upward correction associated with the effects of reabsorption, amounting to 0.1, we arrive at $\gamma=0.8\pm0.2$. The result, within errors equal to unity, indicates that the predominant loss mechanism for near-zone-boundary phonons is removal out of the excited zone by ballistic flight, at least in the case of zone diameters up to about 0.6 mm. Combined with the result for τ_{ZB} of Sec. III A, $\tau_{ZB}=25$ ns at $R=30$ μm, the result implies the intrinsic lifetime of near-zone-boundary phonons to be at least 200 ns.

IV. CONCLUSIONS

With a technique of modulated pumping, which makes it feasible to eliminate the effects of bottlenecked 29-cm^{-1} phonons, it has been demonstrated that the feeding into $2\bar{A}(^2E)$ is substantially larger than the direct optical feeding. The additional feeding per metastable Cr^{3+} is linear in N^*, but becomes quadratic in case the laser wavelength allows for a secondary pumping cycle. The experiments further show the additional feeding to scale approximately with the excited-zone dimensions. These phenomena are explained by a Raman process connecting the $\bar{E}(^2E)$ and $2\bar{A}(^2E)$ populations. The process is induced by near-zone-boundary acoustic phonons produced in the breakup of energy released in the nonradiative decays following the optical excitations. From the analysis, it appeared that occupation numbers per mode of order 10^{-7} are reached at feasible laser powers. The prevailing decay mechanism of the near-zone-boundary phonons is ballistic flight out of the excited zone, at least up to flight paths of 0.3 mm, corresponding to intrinsic lifetimes of over 200 ns. The above study has further demonstrated that the ruby level scheme is selectively sensitive to near-zone-boundary phonons, and hence may be employed as a detector of such phonons.[16]

ACKNOWLEDGMENTS

The work was supported by the Netherlands Foundations Fundamenteel Onderzoek der Materie en Zuiver Wetenschappelijk Onderzoek. The authors are indebted to G. J. Dirksen for crystal growing, C. R. de Kok for technical assistance, and E. H. van Mol for participating in the experiments.

*Present address: Philips Research Laboratories, Eindhoven, The Netherlands.

[1]W. Grill and O. Weiss, Phys. Rev. Lett. **35**, 588 (1975).

[2]P. Hu, V. Narayanamurti, and M. A. Chin, Phys. Rev. Lett. **46**, 192 (1981).

[3]R. G. Ulbrich, V. Narayanamurti, and M. A. Chin, Phys. Rev. Lett. **45**, 1432 (1980).

[4]H. Lengfellner and K. F. Renk, Phys. Rev. Lett. **46**, 1210 (1981).

[5]M. Lax, P. Hu, and V. Narayanamurti, Phys. Rev. B **23**, 3095 (1981).

[6]J. I. Dijkhuis, A. van der Pol, and H. W. de Wijn, Phys. Rev. Lett. **37**, 1554 (1976); J. I. Dijkhuis and H. W. de Wijn, Phys. Rev. B **20**, 1844 (1979).

[7]R. S. Meltzer and J. E. Rives, Phys. Rev. Lett. **38**, 421 (1977); R. S. Meltzer, J. E. Rives, and W. C. Egbert, Phys. Rev. B **25**, 3026 (1982).

[8]K. F. Renk and J. Deisenhofer, Phys. Rev. Lett. **26**, 764 (1971).

[9]S. A. Basun, A. A. Kaplyanskii, and V. L. Shekhtman, Fiz. Tverd. Tela (Leningrad) **24**, 1913 (1982) [Sov. Phys.—Solid State **24**, 1093 (1982)].

[10]J. G. M. van Miltenburg, J. I. Dijkhuis, and H. W. de Wijn (unpublished).

[11]We did not explicitly consider the effects of phonon modes near Van Hove singularities, on the grounds of the smaller densities of states and matrix elements there.

[12]Low-temperature magnetic-susceptibility experiments on these samples yielded concentrations of 90, 500, and 1900 at. ppm, respectively.

[13]R. J. G. Goossens, J. I. Dijkhuis, and H. W. de Wijn, Phys. Rev. B (to be published).

[14]J. E. Rives and R. S. Meltzer [Phys. Rev. B **16**, 1808 (1977)] quote $\phi_{2\bar{A}}/\phi_{\bar{E}}=1/2.6$, or $\phi_{2\bar{A}}=70$ s^{-1}. These authors did not include Raman processes in their analysis, which leads to an overestimate of $\phi_{2\bar{A}}$. A Monteil, B. Champagnon, A. Bogrivent, and E. Duval, presented at the Third International

Conference on Dynamical Processes in the Excited States of Solids, Regensburg, 1981, the result $\phi_{2\bar{A}}/\phi_{\bar{E}}=\frac{1}{19}$, in conformity with ours, by a comparison of the intensity ratios R_2/R_1 upon pumping in $^4T_1$ and $^2T_1$.

[15]W. M. Fairbank, Jr., G. K. Klauminzer, and A. L. Schawlow, Phys. Rev. B 11, 60 (1975).

[16]R. J. G. Goossens, J. I. Dijkhuis, and H. W. de Wijn, J. Lumin. **34**, 19 (1985).